Simultaneous and Rapid Removal of Safranin O (SO) and Basic Blue 41 (BB) Dyes by Sulfonated Polyacrylamide (PAA-SO3H) As Super-Adsorbent, Isotherms, and Kinetics Studies

Mohammad Ali Zare (m.a.zare@miau.ac.ir)
Islamic Azad University Marvdasht https://orcid.org/0000-0003-0655-6440
Zahra Jamali
Islamic Azad University Marvdasht
Abdoulhamid Fadavi
Islamic Azad University Marvdasht
Reza Sanaye
Shiraz Medical School: Shiraz University of Medical Sciences
Maryam Iranpour
Islamic Azad University Shiraz

Research Article

Keywords: Super-Adsorbent, Safranin O, Basic blue 41, Removal, Isotherm models, Kinetic models

Posted Date: March 9th, 2021

DOI: https://doi.org/10.21203/rs.3.rs-174770/v1

Simultaneous and rapid removal of Safranin O (SO) and Basic blue 41 (BB) dyes by sulfonated polyacrylamide (PAA-SO_3H) as super-adsorbent, isotherms, and kinetics studies

Mohammad Ali Zare*[1] ● Zahra Jamali[1] ● Abdoulhamid Fadavi[1] ● Reza Sanaye[2] ● Maryam Iranpour[3]

Abstract The goal of this piece of research would be delving into the nature of simultaneous ultrasound removal of SO and BB dyes into solutions by means of sulfonated polyacrylamide as an efficient adsorbent. Sulfonated polyacrylamide has been synthesized and fully described, applying FT-IR technique. The percentage level of dye removal was investigated under several factors such as the time of sonicating, initial concentrations of dye, pH, and adsorbent dosage. Optimization of parameters was conducted using central composite design (CCD) with response surface methodology (RSM). An acceptable degree of consonance between experimental and calculated values was arrived at. High percentage removal (90.0% and 99.9%) of SO and BB in short time (2.16 min) were recorded through the application of an ultrasound-assisted adsorbent (0.008g).

Keywords Super-Adsorbent ● Safranin O ● Basic blue 41 ● Removal ● Isotherm models ● Kinetic models

✉ Mohammad Ali Zare

E-mail: M.A.Zare@miau.ac.ir

Phone Number: +9809171001708

Fax Number: +987143311172

[1] Department of Chemistry, Marvdasht Branch, Islamic Azad University, Marvdasht, Iran.

[2] Department of Medical Nanotechnology, School of Advanced and Technologies, Shiraz University of Medical Sciences.

[3] Department of chemistry, Shiraz Branch, Islamic Azad University, Shiraz, Iran.

1 Introduction

There is a relatively wide spectrum of differing pollutants affecting life, of which the two main sources are environmental pollution and human pollution. One of the most significant sources of environmental pollution is sewage coming from industries such as textiles, leather, cytology, printing, food etc.; these apply pigments and dyes in the manufacturing of their final products. The rest of the dyes have the capability to interfere with aquatic life and even to contaminate the food chain. Furthermore, the greater part of the harm arises from the fact that some dyes cause allergy, skin disturbance, irritation, cancer, and even mutation in humans (Mullerova et al. 2019). Consequently, dyes undoubtedly represent a genuine danger not only to water environment but also human health (An et al. 2020). This is because such dyes possess characteristics of persistent, extremely visible, non-biodegradable nature; this is over and above the fact that they are mostly stable to oxidizing agent and sunlight (Regti et al. 2017; Mahmoodi and Abdi 2019; Tan and Sen 2020). Thence, the necessity for the dye-containing water is to undergo treatment prior to any disposal to the environment (Mahmoodi and Abdi 2019).

It has been estimated that something more than 700,000 t of dyestuff produced per year, in addition to the very available dyes are emitted into the environment while no truly proper treatment has been exerted on them (Shariati et al. 2011). As a result, there is real necessity to remove these from industrial effluents for purposes of creating a healthy purified aqueous environment. It ought to be noted that the said dyes have some structural diversity—their removal is laborious during the waste water treatment.

In order to eliminate pollutants from wastewater, adsorbents can be introduced as an efficatious and simple method. Several materials such as agricultural wastes, natural compounds, activated carbon, etc. may be made use of as adsorbents. For the simple fact that contaminants are generally removed in an indiscriminant manner, there are many problematic as for selective recovering of the same contaminants to reuse them. Those adsorbents which are produced on the basis of cheap materials are, of course, attractive with many practical applications. Nonetheless, there is immense need to expand the improvement of adsorption capacities, mechanical strength, uncomplicated designing, flexibility, ease of operation (Mahmoodi 2011; Noroozi and Sorial 2013; Tan and Sen 2020).

Adsorbents that have polymeric shapes have appeared as sort of a potential remedy to commonly traditional adsorbents. Their efficiency manifests itself as for huge surface area, fully mechanical stiffness, controlled

variable surface chemistry, pore size distribution, and feasible regeneration on the basis of mild states (Pan et al. 2009).

Design according to a methodology of experiential platform causes the evaluating over the main and the combination (interaction) influences on the part of variables in minimum states of experiments (Pizarro et al. 2012).

The synthesis of sulfonated polyacrylamide was followed by its characterization by means of FT-IR techniques. The SO and BB retrieval from solutions was remarkably accelerated as ultrasonic instrument was brought in to rapidly assist the adsorption method. This was detected by UV-Vis spectrophotometer. Next to the pH optimization, the time period of sonicating and initial SO and BB concentrations in addition to the dosage of adsorbent were all examined and actually improved through the medium of Central Composite Design (CCD) with Response Surface Methodology (RSM) by the Desirability Function (DF). The data gained experimentally were fitted to conventional kinetic modeling, including pseudo first and second-order besides intra-particle diffusion models, and so the adsorption was assayed.

2 Experimental

2.1 Instruments and reagents

5.00 mg of each solid dyes of BB and SO in 0.1 L double distilled water were dissolved and the stock solution (0.5 g/L) of them were prepared and the needed concentrations daily were produced by their proper dilution.

The pH measurements were performed by pH meter (Metrohm, model 827, Switzerland) and the BB and SO concentrations were measured by UV-Vis spectrophotometer (Perkin-Elmer, Lambda 45, USA) and a glass cell with an optical part (1.000 cm at wavelengths of 664.7 and 520.0 nm for BB and SO, respectively). An ultrasonic instrument (model LBS2) at frequency 40 KHz and 285W was used for the ultrasound- adsorption procedure. pH Effect on the performance of adsorption was studied between pHs 2-10. pH of dyes was maintained by 0.1 F Sodium hydroxide and Hydrochloric acid solution.

2.2 Ultrasound- adsorption method

The ultrasound can simultaneously remove BB and SO, and can accelerate this. In the ultrasonic device, which contained 2.5 L water, constant temperature during the experiment was hold. The experiment of sono-chemical adsorption was carried out: determined amounts of 400.0 mg/L of BB and SO solution (50 mL) were mixed with 0.01g of PAA-SO_3H under ultrasound radiation over 3 min at room temperature. At the end, the samples were rapidly centrifuged and non-retained BB and SO contents were evaluated according to the calibration curve at the same condition.

2.3 Synthesis of sulfonated polyacrylamide (PAA-SO_3H)

In a 200 mL round-bottom flask, 5.00 g Acryl Amide (70 mmol), 5.17 g 2-acrylamido-2-methylpropansulfonic acid (AAMP) (25 mmol) and 0.77 g N,N'-methylenebisacrylamide (NNMBA) (5 mmol) were dissolved in approximately 100 mL ethanol. 125 mg Benzoyl peroxide (0.5 mmol) was added to them and the mixture was heated while stirring at reflux state for 5 h. Using filtration, the resulted polymer was collected and washed three times with hot ethanol and dried at 70 °C under reduced pressure overnight. Dried polymer weight was 10.10 g which is 91.8% gravimetric yields (Schematic 1). Back titration method also showed a 1.1 mmol/g polymer acidic capacity. This is equivalent to 91% titrimetric yield (Khodadoust and Hadjmohammadi 2011).

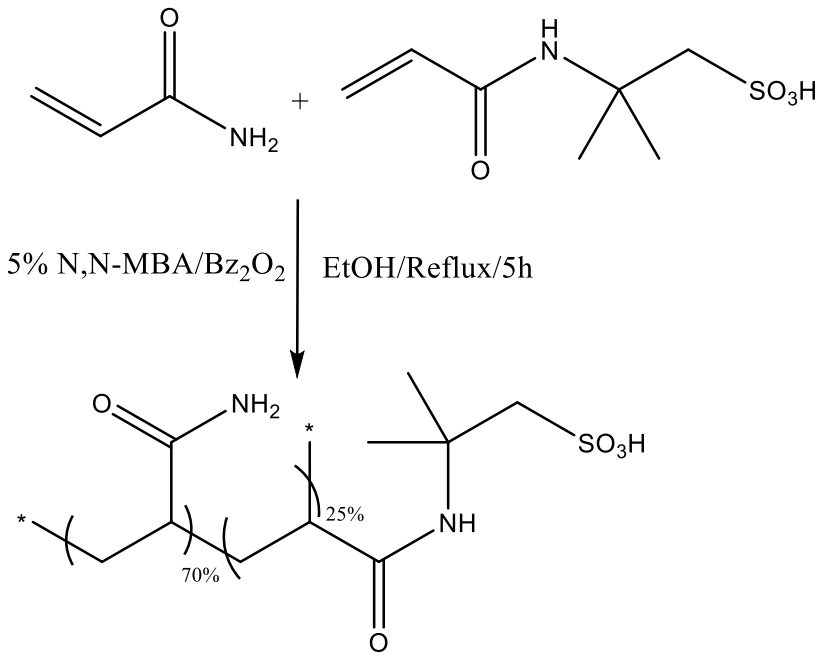

5% Crosslinked Sulfonated polyacrylamide or (PAA-SO_3H)

Schematic 1 Preparation of sulfonated polyacrylamide via transamidation reaction

2.4 dye uptake measurements

The concentrations of dye were measured based on the plots of calibration achieved at the equal conditions. The removal values of BB and SO (RE%) were determined using the following Equation. (1):

$$RE\% = \left(\left(C_0 - C_e \right) / C_0 \right) \times 100 \quad (1)$$

where, C_0 (mg/L) and C_t (mg/L) are the target concentrations at initial and next time t, respectively. The adsorbed BB and SO amounts (q_e (mg/g)) were calculated as follows (i.e., mass balance relationship):

$$q_e = (C_0 - C_e)V/W \quad (2)$$

where, C_0 and C_e (mg/L) are the initial and equilibrium dye concentrations in aqua, respectively, V (L) is the solution volume and W (g) is the adsorbent mass.

3 Result and discussion

3.1 FT-IR spectra for PAA-SO_3H adsorbent of SO and BB and adsorbed SO and BB on PAA- SO_3H

FT-IR (KBr) spectrum of the prepared PAA-SO_3H adsorbent is presented in Fig. 1c. Absorption peaks around 3536-3182 cm^{-1} indicates the N–H stretching mode of amino groups. The peak at 1682 cm^{-1} indicates the C=O stretching vibration in amide groups. Peaks at 1444 cm^{-1} and 1182 cm^{-1} and 1038 cm^{-1} indicates the S=O stretching vibration in sulfonate groups. For the BB Fig. 1b, the peak at 3486 cm^{-1} indicates the OH stretching vibration. The peak at 2375 cm^{-1} shows the N=N stretching vibration in azo group. The peak at 1569 cm^{-1} shows the C=N stretching vibration. Following the adsorption of BB onto PAA-SO_3H, two new peaks were seen in 2358 and 1596 cm^{-1} (Fig. 1a), which can be simultaneous with the absorption of BB. Therefore, BB has been anchored on the surface of PAA-SO_3H structures when the adsorption process is carrying out.

FT-IR (KBr) spectrum of the prepared PAA-SO_3H adsorbent is presented in Fig. 1f. Absorption peaks around 3536-3182 cm^{-1} shows the N–H stretching mode of amino groups. The peak at 1682 cm^{-1} indicates the C=O stretching vibration in amide groups. Peaks at 1444 cm^{-1} and 1182 cm^{-1} and 1038 cm^{-1} shows the S=O stretching vibration in sulfonate groups. The peak for the SO Fig. 1e at 3330 cm^{-1} indicates the OH stretching vibration. The peak at 2368 cm^{-1} shows the N=N stretching vibration in azo group. Peaks at 1334 cm^{-1} and 1194 cm^{-1} and 1016

cm^{-1} shows the S=O stretching vibration in sulfonate groups. Following the adsorption of SO onto PAA-SO_3H, two new peaks were observed in 2378 and 1522 cm^{-1} (Fig. 1d), which can be during the absorption of SO. Therefore, SO was fixed on the surface of PAA-SO_3H structures when the adsorption process was carrying out (Li et al. 2010; Deng et al. 2011).

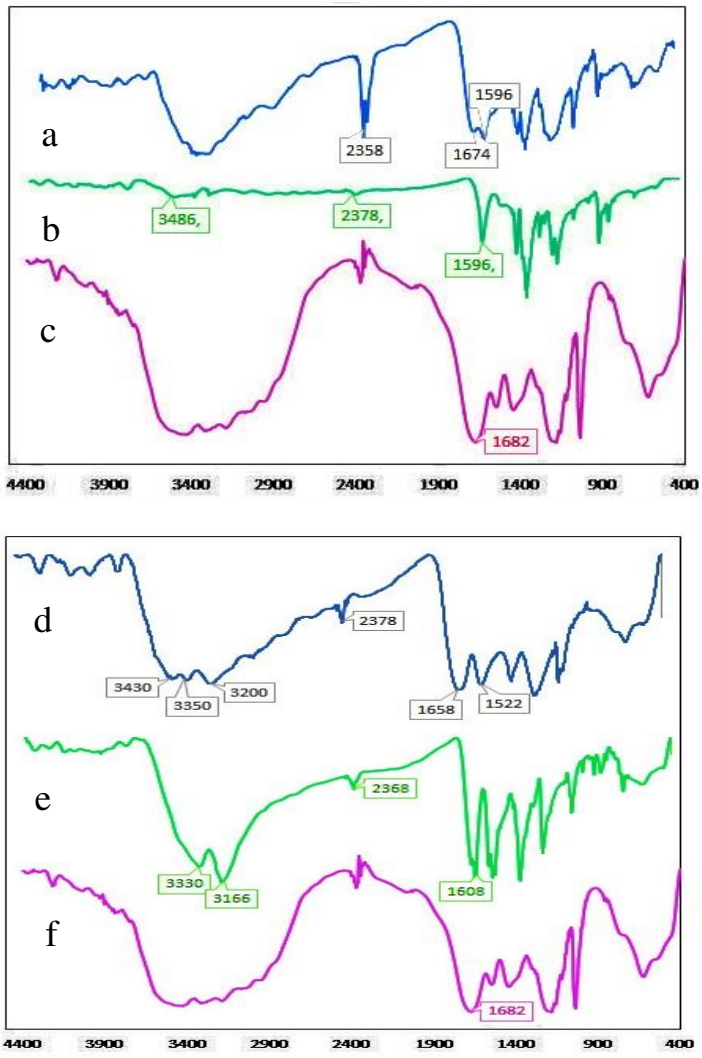

Fig. 1 FT-IR (KBr) for the developed adsorbent. (a) adsorbed BB on PAA- SO_3H (b) BB, (c) PAA- SO_3H adsorbent, (d) adsorbed SO on PAA- SO_3H (e) SO, (f) PAA- SO_3H adsorbent.

3.2 Central Composite Design (CCD)

Generally, experimental design can simultaneously cause the optimizing effects of variables to optimize performance and decrease error with minimum experimental runs (Martins et al. 2012; Saeid and Mehrorang 2013). In this research, the Central Composite Design (CCD) as optimizing model with broad application allows the estimating coefficients as mathematical type and predict the response, and the predicted model validation was

used for optimizing the removal amounts (%) of BB and SO dyes. The experimental design points with variables coded values in experiment matrix (-2, -1, 0, +1, +2) consists of 2n factorial points (n: number of variables), 2n axial points and Nc central points (Nc = 5) that are presented in Table 1. The design matrix and the responses are presented in Table 2.

The experimental error and the reproducibility of the data were determined using the center points. Using the second order polynomial model, the mathematical relationships between the three independent variables can be estimated (LeFevre 2000; Hossain et al. 2012):

Table 1

Design matrix for the 2^5 central composite designs

Variables	Levels			Star point = 2	
	Low (-1)	Central (0)	High (+1)	-α	+α
(X_1) SO concentrations (mg/L)	350.0	400.0	450.0	300.0	500.0
(X_2) BB concentrations (mg/L)	350.0	400.0	450.0	300.0	500.0
(X_3) pH	4.00	6.00	8.00	2.00	10.00
(X_4) amount of adsorbent (g)	0.008	0.01	0.012	0.006	0.014
(X_5) sonication time (min)	2	3	4	1	5

Table 2

Experimental conditions and values obtained through the CCD

Runs	X_1	X_2	X_3	X_4	X_5	%RE SO	%RE BB
1	400.0	400.0	6.00	0.010	5.00	86.51	87.01
2	400.0	400.0	6.00	0.010	3.00	73.02	84.39
3	400.0	400.0	6.00	0.010	3.00	78.32	83.48
4	350.0	350.0	8.00	0.012	4.00	82.69	87.62
5	400.0	400.0	2.00	0.010	3.00	56.94	53.76

6	500.0	400.0	6.00	0.010	3.00	59.44	78.42
7	400.00	400.0	6.00	0.010	1.00	70.97	83.05
8	450.0	350.0	8.00	0.012	2.00	72.65	78.62
9	450.0	450.0	4.00	0.008	4.00	66.28	75.42
10	400.0	400.0	6.00	0.010	3.00	76.94	83.20
11	300.0	400.0	6.00	0.010	3.00	84.50	90.71
12	450.0	350.0	4.00	0.012	4.00	78.22	88.75
13	350.0	450.0	4.00	0.012	4.00	78.21	77.65
14	350.0	350.0	4.00	0.008	2.00	70.87	80.67
15	400.0	400.0	6.00	0.010	3.00	78.29	83.92
16	450.0	450.0	8.00	0.008	2.00	73.62	69.54
17	400.0	400.0	6.00	0.014	3.00	85.15	86.45
18	400.0	400.0	6.00	0.010	3.00	75.19	84.55
19	350.0	450.0	8.00	0.008	4.00	78.69	80.31
20	400.0	300.0	6.00	0.010	3.00	81.96	95.01
21	450.0	450.0	4.00	0.012	2.00	85.89	89.62
22	350.0	450.0	8.00	0.012	2.00	60.90	82.88
23	400.0	400.0	6.00	0.006	3.00	75.29	73.39
24	400.0	500.0	6.00	0.010	3.00	69.75	84.58
25	400.0	400.0	10.00	0.010	3.00	78.66	84.25
26	450.0	350.0	8.00	0.008	4.00	82.12	79.22

Abbreviations: %RE: removal percentage

163

$$y = \beta_0 + \sum_{i=1}^{3} \beta_i \chi_i + \sum_{i=1}^{3} \sum_{j=1}^{3} \beta_{ij} \chi_i \chi_j + \sum_{i=1}^{3} \beta_{ii} \chi_i^2 \quad (3)$$

where, y is the calculated response (removal percentage) in Equation (3); X_i's are the independent variables (time of sonicating, SO and BB concentrations and amount of adsorbent). The β_0 is the constant in model; β_i is the linear coefficient; β_{ii} is the quadratic coefficient and β_{ij} is the cross-product coefficient.

The complete design was randomly performed to minimize the effects of non-controlled variables. This design can approximately estimate the main, interaction and quadratic effects. Then, RSM was produced based on all the significant interactions in the CCD for optimizing the critical factors and explaining the nature of the response surface.

The removal plots (%) versus significant variables as pair factors at fixed and optimum values of other variables were represented. These curvatures of plots show the interaction between the variables. The ANOVA and regression coefficients explain the significant ($p < 0.05$) nature of contribution of the quadratic model. The lack of fit (LOF) is the variation of the data around the fitted model. LOF is a certain test for model fit adequacy and without the effects of the additional higher-order terms Table 3. The non-usefulness of this model for fitting the data causes the significant value. The p-value of LOF were 0.675 for SO and 0.131 for BB that approve the good importance of this model for well-fitting the response. The terms x_1; x_2; x_3; x_4; x_5; x_1x_2; x_1x_4; x_2x_3; x_3x_4 and x_3x_5 were significant for the SO removal. Which means that the time, adsorbent dosage and SO concentration linearly and quadratically affect the SO removal. The interaction of the time and adsorbent dosage is also effective on the response. For the BB removal, the terms x_1; x_2; x_3; x_4; x_5; x_1x_2; x_1x_3; x_1x_4; x_1x_5; x_2x_2; x_2x_3; x_2x_4; x_2x_5; x_3x_4 and x_3x_5 were significant. It means that the time, adsorbent dosage, concentration of BB is linearly and quadratically effective on the response. The optimized values for the factors of pH, adsorbent dose, SO and BB concentrations and contact time were 7.90, 0.008 g, 362.0 mg/L, 420.4 mg/L and 2.16 min, respectively. At this condition, the removal value (%) for each dye was predicted by 99.8% with desirability 0.999, see Fig. 2. For testing the reliability of this prediction, an experiment was run at the obtained optimum condition and the removal percentage of each dye. Response surface methodology (RSM) is used for determination and evaluation of the relative significant of parameters and solving the multivariate equation with an optimum response. The modeling was carried out by adjusting first or second order polynomials equations to the experimental responses. Then, the results were examined by variance analysis (ANOVA) to identify main effects of and interactions of variables. The tridimensional graph plotting leads to generate the surface response for predicting the best operating conditions based on p-value and F-value.

193 $\%\ R\ SO = +700.49 - 23.05X_1 - 12.72X_2 + 54.48X_3 - 15096.91X_4 + 13.55X_5 + 0.38X_1X_2 + 684.08X_1X_4 -$

194 $0.52X_2X_3 - 2496.04X_3X_4 - 2.29X_3X_5 - 0.51X_3^2 + 2.63E+005\ X_4^2$ (4)

195

196 **Table 3**

197 Variance analysis for the removal of BB (%R)

Source	Sum of Squares	df	Mean Square	F Value	P value (Prob>F)
Model	1565.18	20	78.26	18.23	0.0022
X_1	314	1	314	73.14	0.0004
X_2	74.54	1	74.54	17.36	0.0088
X_3	235.88	1	235.88	54.94	0.0007
X_4	48.61	1	48.61	11.32	0.02
X_5	120.75	1	120.75	28.12	0.0032
X_1X_2	313.48	1	313.48	73.02	0.0004
X_1X_3	10.78	1	10.78	2.51	0.1739
X_1X_4	158.66	1	158.66	36.95	0.0017
X_1X_5	28.24	1	28.24	6.58	0.0504
X_2X_3	92.53	1	92.53	21.55	0.0056
X_2X_4	1.61	1	1.61	0.37	0.5675
X_2X_5	4.77	1	4.77	1.11	0.3399
X_3X_4	337.96	1	337.96	78.72	0.0003
X_3X_5	71.4	1	71.4	16.63	0.0096
X_4X_5	25.07	1	25.07	5.84	0.0604
X_1^2	27.85	1	27.85	6.49	0.0515
X_2^2	0.039	1	0.039	9.08E-03	0.9278
X_3^2	115.14	1	115.14	26.82	0.0035
X_4^2	30.36	1	30.36	7.07	0.0449
X_5^2	12.78	1	12.78	2.98	0.1451
Residual	21.47	5	4.29		

Lack of Fit	1.04	1	1.04	0.2	0.6752
Pure Error	20.43	4	5.11		
Cor Total	1586.65	25			

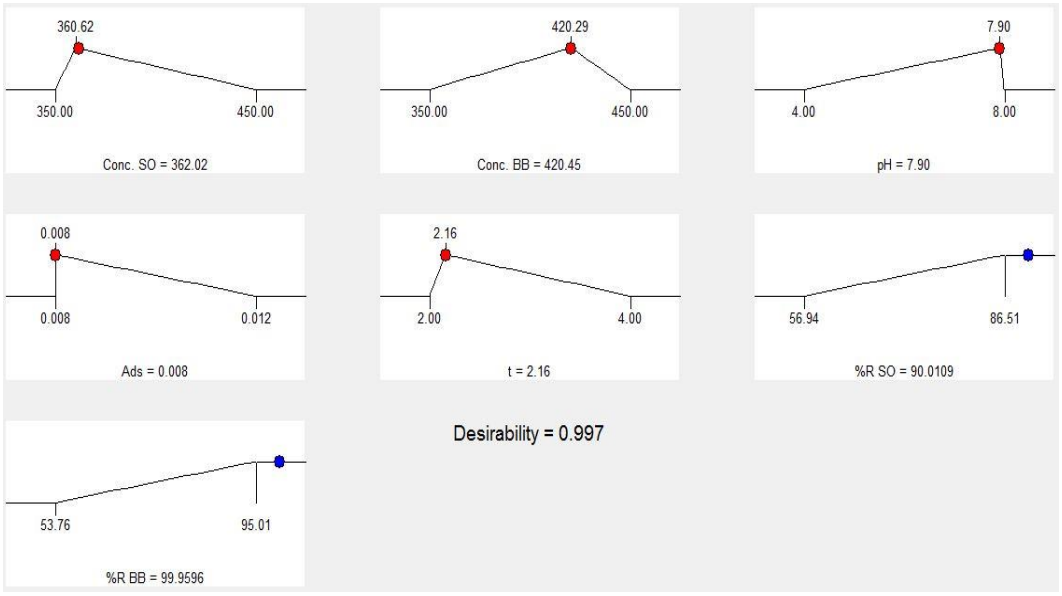

Fig. 2 Optimization plot of factors.

3.3 Response Surface Methodology

Subsequently, RSM was developed by considering all the significant interactions in the CCD to optimize the critical factors and describe the nature of the response surface in the experiment (Fig. 3). In these three-dimensional diagrams, the dependent parameters on the X, Y axes, and the response on the axis Z was plotted (the values of the other parameters in each diagram are fixed in the optimal value). Fig. 3a shows the simultaneous effect of SO concentrations and adsorbent dosage on the percentage of BB removal by the adsorbent. The results indicated that low levels of SO and increase the adsorbent dosage in solution will increase the amount of BB ion removal and adsorption.

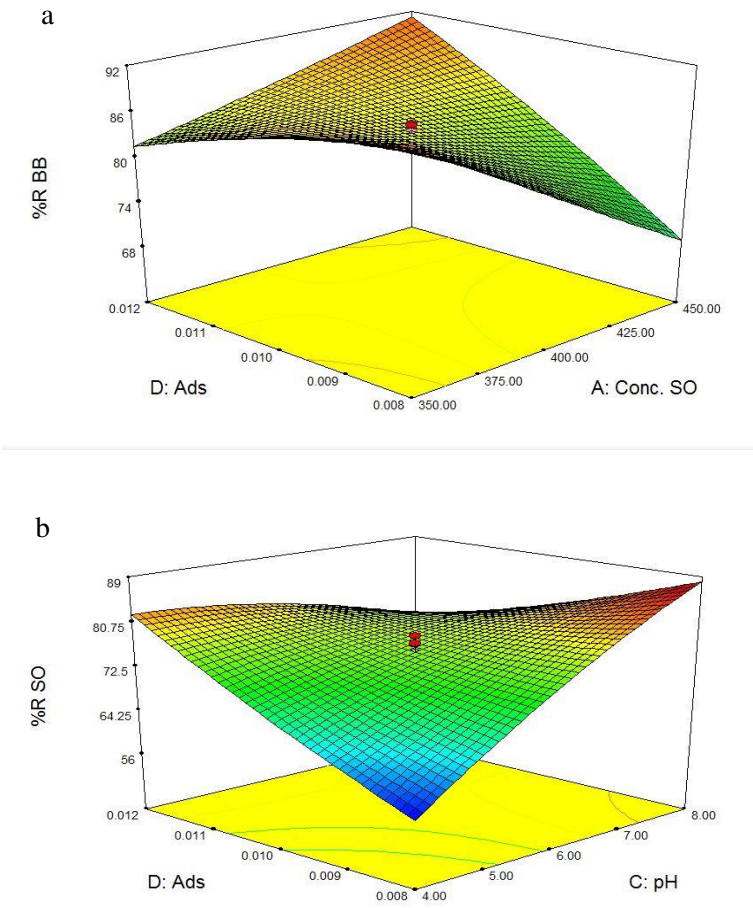

Fig. 3 Response surfaces for the 2^5 central composite designs for simultaneous of SO and BB. a) SO concentration and adsorbent, (b) pH and adsorbent.

3.4 Study of equilibrium absorption isotherms

Isotherm models are used to provide an insight into the absorption mechanism, surface properties, adsorbent tendency, and descriptions of absorption experimental data. Several adsorption equilibrium isotherms that are widely used to analyze equilibrium data of solute between adsorbent and solution in solid systems are Langmuir, Freundlich, Tempkin and Deboning–Radushkevich (D–R) isotherms. These isotherm models were used to fit the experimental data in the present study.

3.4.1 The Langmuir isotherm

This isotherm (Langmuir 1918) is widely used for modeling equilibrium data. The Langmuir model was assumed that sorption occurs in a monolayer, surface is homogeneous and there is no interaction between adjacent adsorbed molecules. In this model, the linear equation is represented by the following equation:

$$C_c/q_e = 1/K_a Q_m + C_e/Q_m \quad (5)$$

The linear plots of C_e/q_e versus C_e suggest the applicability of the Langmuir isotherm in Table 4. The correlation coefficients reported in the Table 4 demonstrated powerful positive evidence on the adsorption of the SO and BB onto the PAA-SO_3H using the Langmuir model.

3.4.2 The Freundlich isotherm

One of the most common models to describe adsorption isotherms is the Freundlich isotherm (Freundlich 1906). This model describes a reversible adsorption of multilayers of adsorbed molecules in a heterogeneous system. The well-known linear form of the Freundlich isotherm is represented by the empirical equation:

$$Lnq_e = LnK_f + (1/n)LnC_e \quad (6)$$

where, q_e is the amount of the adsorption SO and BB (mg/g), C_e is the equilibrium concentration of SO and BB in the solution (mg/L). K_f and 1/n are the Freundlich equilibrium and adsorption constant, respectively. K_f indicative of adsorption capacity of PAA-SO_3H and 1/n show adsorption intensity in Table 4. The reasonable correlation coefficients (0.988–0.993 for PAA-SO_3H) indicates its higher efficiency for the interpretation of experimental data than the Langmuir isotherm. 1/n value changes when the mass of adsorbent from 0.539 to 0.475 raised. The K_f has increased with adsorbent mass from 145.525 to 232.273. It indicates that the adsorption capacity of the adsorbent raised in a unit equilibrium concentration for adsorption of more species.

3.4.3 The Tempkin isotherm

Another empirical equation that study the absorption processes is the Tempkin model. This isotherm expresses the adsorption mechanism with an adsorbent– adsorbate interaction. The isotherm is given by the following equations Equation (7) (Aharoni and Ungarish 1977):

$$q_e = RT/b\, LnAC_e \quad (7)$$

This isotherm was simplified as follows (Tempkin and Pyzhev 1940; Akkaya and Özer 2005):

$$q_e = \beta Ln\alpha + \beta LnC_e \quad (8)$$

R= Ideal gas constant (8.314 J/(mol/K))

b_T= Temkin isotherm constant

β=Constant related to heat of sorption (J/mol)

T= Temperature at 298K.

When the experimental equilibrium data were fitted to the above-mentioned equation revealed the high and reasonable applicability of this isotherm to interpret and explain the SO and BB adsorption onto PAA- SO_3H in Table 4.

3.4.4 The Deboning–Radushkevich (D–R) isotherm

A useful empirical theory that express the adsorption mechanism with a Gaussian energy distribution onto a heterogeneous surface is D–R isotherm (Dubinin 1960, 1965). The non-linear and linear equation can be illustrated Equation (9) and Equation (10) respectively:

$$q_e = Q_m \exp\left(-K\varepsilon^2\right) \quad (9)$$

$$Lnq_e = LnQ_m - K\varepsilon^2 \quad (10)$$

where, Q_m is the theoretical saturation capacity K_{DR} ($mol^2/(KJ^2)$) is related to free energy of adsorption and ε is the Polanyi potential that can represented by Equation (11):

$$\varepsilon = RTLn\left(1 + 1/C_e\right) \quad (11)$$

Based on Equation (10), plotting Ln q_e versus ε^2 enables to be determine as K ($mol^2/(kJ)^2$) and adsorption capacity (Q_m (mg/g)) through the interception and the slope values, respectively.

The K gives the mean free energy (E) of sorption per molecule of the sorbate from infinity in solution to the solid surface can be illustrated as Equation (12) (Radushkevich 1949)

$$E = 1/\sqrt{2K} \quad (12)$$

The estimated values of D–R parameters are given in Table 4 The model saturation adsorption capacity at optimum states by adsorbents in the range of 0.008–0.01 g, respectively has proper agreement with the relative Langmuir value (20000 for SO and 8333.4 mg/g for BB).

3.5 Adsorption kinetics

In this study, several Kinetic models and their parameters have been used to describe and predict adsorption data and potential rate controlling steps, which are helpful for the prediction of adsorption rate, describe the kinetic process of adsorption and give important information for designing and modeling the adsorption processes. Here we used four widely-used kinetic models to investigate the processes of the simultaneous adsorption of SO and BB on the PAA-SO_3H. Therefore, the mentioned models are discussed in the following sections.

The rate of adsorption in pseudo-first-order model (LAGERGREN and S. 1898) is based on the adsorption capacity and generally expressed as follows Equation (13):

$$Ln(q_e - q_t) = Lnq_e - K_1 t \quad (13)$$

where, q_e and q_t are the amount of the SO and BB on the PAA-SO_3H surface at equilibrium and at time t (mg/g), respectively. k_1 is the pseudo-first order rate constant (L/min). By this equation, the plot of first order model log (q_e -q_t) versus t for the adsorption of SO and BB concentration on the PAA-SO_3H C_0= 350.0 (mg/L) at 25^0C show that the correlation coefficient (R^2) for each dye is 0.918 and 0.924, respectively and comparatively low for most adsorption data and another concentration (C_0= 450.0 (mg/L)). Therefore, the reaction mechanism for adsorption of SO and BB on the PAA-SO_3H surface is inappropriate. Then, kinetic data are fitted with another model (Weber and Morris 1963; Aharoni and Ungarish 1977). The adsorption kinetic can be described by the pseudo-second order model (Ho and McKay 1999) and may be expressed in the form:

$$t/q_t = 1/K_2 q_e^2 + t/q_e \quad (14)$$

The curve fitting plot of log (q_e - q_t) versus t does not show good results for the entire adsorption period. The kinetic data such as k_2 and equilibrium adsorption capacity, q_e, for the adsorption of SO and BB onto PAA-SO_3H surface were calculated based on the intercept and slope of the plot of t/q_t versus t, respectively in Table 5. The values of correlation coefficients R^2, is closer to unity (0.999) for the pseudo-second-order kinetic model for all initial dye concentrations (350.0 mg/L and 450.0 mg/L), as presented in Table 5. This shows that the adsorption

mechanism of PAA-SO_3H obeys the pseudo-second-order kinetic model for the entire adsorption period. Also, with increasing initial concentration SO and BB, the diffusion rate enhancement and the value of k_2 increased.

One of the most useful kinetic model to evaluate the adsorption process is the Elovich equation (Aharoni and Ungarish 1977). This equation is expressed as follows according to the adsorption capacity:

$$q_t = 1/\beta\, Ln(t) + 1/\beta\, Ln(\alpha\beta) \quad (15)$$

Important parameters, such as Elovich maximum adsorption capacity and Elovich constant can be calculated from the slope and intercept of the equation of Equation (15) and reported in Table 5.

Another kinetic model that evaluate the adsorption process is Intra-particle diffusion (Thompson and Doraiswamy 1999; Chakma and Moholkar 2011). In this process, SO and BB may be transported and movement from the bulk of the solution to the adsorbent (PAA-SO_3H) by intra-particle diffusion. Therefore, the intraparticle diffusion model has been used to study the rate-limiting step for the adsorption of both dyes onto PAA- SO_3H surface. A general equation indicates the intra-particle diffusion model as follows:

$$q_t = K_{id} t^{1/2} + C \quad (16)$$

The values of k_{id} and C are determined using the slope and intercept of the plot of q_t versus $t^{1/2}$, respectively in Table 5. C and k_{id} are constant and intra particle diffusion rate constant, respectively. If the plot of q_t versus $t^{1/2}$ passes through the origin, intra-particle diffusion alone is the rate limiting step (Midathana and Moholkar 2009). Based on the obtained data in Table 5, The R^2 value for this kinetic model was far from the unity. This show that the intra-particle diffusion model cannot be appropriate. As a final result and R^2 values obtained, we concluded that pseudo-second-order kinetic model for the SO and BB removal over entire sorption period is understood (Maddikeri et al. 2012).

Table 4

Isotherm constant of SO and BB on PAA-SO_3H at optimum condition.

Isotherm	Parameters	Adsorbent (g)			
		0.008		0.01	
		SO	BB	SO	BB

Langmuir	Q_m (mg/g)	20000	8333.4	11111.2	5263.2
	K_a (L/mg)	0.0096	0.00012	0.0012	0.0067
	R^2	0.988	0.9646	0.826	0.985
Freundlich	1/n	0.78	0.5398	0.782	0.475
	K_F (L/mg)	302.0	154.5	32.2	232.2
	R^2	0.995	0.988	0.991	0.993
Tempkin	B_l	3246.2	1828.3	1761.1	1205
	K_T (L/mg)	7.04	40.4	57.7	16.5
	R^2	0.991	0.968	0.962	0.983
Dubinin and Radushkevich	Q_s (mg/g)	6272.9	4591.6	3245.4	3124.4
	B	-3E-5	-0.0015	0.0018	-0.00035
	E (kJ/mol)	129.0	3.3	16.6	37.8
	R^2	0.908	0.813	0.830	0.860

Table 5

Kinetic parameters of SO adsorption onto PAA- SO_3H (0.008g of adsorbent, 350.0 and 450.0 mg/L for SO to BB concentration ratio at optimum conditions of other variables)

Model	Parameters	Concentration dye			
		350.0 (mg/L)		450.0 (mg/L)	
		SO	BB	SO	BB
First order kinetic model	K_1	0.931	0.9094	0.956	0.941
	q_e(calc)	195.1	113.7	188.6	118.6
	R^2	0.918	0.924	0.951	0.957
Second order kinetic model	K_2	0.027	0.0428	0.031	0.044
	q_e (calc)	181.8	204.08	222.2	256.4
	h	909.0	1785.71	1550.6	2941.1
	R^2	0.999	0.999	0.999	0.999

Intraparticle diffusion	K_{diff}	54.89	34.65	61.69	46.97
	C	1959.9	2058.3	2510.4	2633.6
	R^2	0.993	0.939	0.899	0.796
Elovich	β	0.0275	0.0437	0.0235	0.0302
	R^2	0.972	0.919	0.954	0.885

Table 6 compares several reported adsorbents for dyes removal from aqueous solutions. The adsorption capacity of dyes onto PAA-SO_3H is higher than or comparable with previously reported adsorbents.

Table 6

Comparison of adsorption capacity of different adsorbents for removal SO and BB

Adsorbents	Adsorbate	Adsorption capacity ($mg.g^{-1}$)	Reference
Macroalgae Cymopolia barbata biomass	Safranin O	192.2	(Mullerova et al. 2019)
Egyptian ferruginous kaolinite	Safranin O	59.3	(Abukhadra et al. 2020)
MgO decked FLG coated Fuller's earth	Safranin O	201.1	(Reddy et al. 2018)
Zinc oxide nanorod-loaded activated carbon	Safranin O	32.06	(Sharifpour et al. 2018)
Modified pine cone powder	Safranin O	208	(Ashrafi et al. 2018)
Lignin nanoparticle	Safranin O	99	(Azimvand et al. 2018)
Lignin Nanoparticle-G-Polyacrylic Acid		138.88	
Sodium Alginate Graft Copolymer	Safranin O	23.98	(Shelar-Lohar and Joshi 2019)
Mesoporous Graphite Functionalized	Safranin O	20.66	(Shaban et al. 2018)

PAA-SO_3H	Safranin O	**20000**	Present study
Persea americana-activatedcarbon	Basic Blue 41	625	(Regti et al. 2017)
Zeolite	Basic Blue 41	39	(Gougazeh et al. 2019)
Activated carbon prepared from filamentous algae	Basic Blue 41	125	(Afshin et al. 2018)
Effective Microorganisms	Basic Blue 41	456.8	(Pushpa T et al. 2019)
Waste Bricks	Basic Blue 41	60	(Kooli et al. 2019)
Pineapple leaf	Basic Blue 41	52.6	(Kamaru et al. 2016)
Zeolitic tuff	Basic Blue 41	192.31	(Humelnicu et al. 2017)
PAA-SO_3H	Basic Blue 41	**8333.4**	Present study

Conclusions

The synthesis of PAA-SO_3H had been carried out and used as a novel adsorbent to rapid individually and simultaneously adsorb of SO and BB. The optimum and best condition for the factors of pH, adsorbent dose, SO and BB concentrations and contact time were 7.90, 0.008g, 362.02 and 420.45 mg/L and 2.16 min, respectively. At this state, the removal percentage of SO and BB calculated by 99.9%. A quick adsorption process (2.16 min) using PAA-SO_3H is so expected for important adsorption usages. An empirical explanation of a competitive Freundlich model was proposed to calculate the simultaneous adsorption of SO and BB. Four Conventional kinetic models were used, and it seems that pseudo-second order equation is proper for fitting the empirical data. It is shown that the pseudo-second-order model has proper fitting with the adsorption data for both dyes. Several isotherm models were investigated to explain the experimental data and their parameters, and also correlation coefficients were determined. Freundlich model shows the proper agreement with the experimental data of both dyes, and the maximum adsorption capacities were **20000** and **8333.4** mg/g for SO and BB, respectively.

Declarations

Ethics approval and consent to participate

Not applicable

Consent for publication

Not applicable

Availability of data and materials

The databases used and/or assessed during the present analysis are accessible from the corresponding author on reasonable request.

Conflict of interest

The authors declare that they have no known competing financial interests or personal relationships that could have appeared to influence the work reported in this paper.

Funding

Not applicable

Authors' contributions

Ideas: Abdolhamid Fadavi; Literature search: Zahra Jamali; Data analysis: Maryam Iranpour; Writing—original draft preparation: Zahra Jamali; Writing—review and editing: Reza Sanaye; Critically revised: Mohammad Ali Zare.

References:

Abukhadra MR, El-Meligy MA, El-Sherbeeny AM (2020) Evaluation and characterization of Egyptian ferruginous kaolinite as adsorbent and heterogeneous catalyst for effective removal of safranin-O cationic dye from water. Arab J Geosci 13:169

Afshin S, Mokhtari SA, Vosoughi M, et al (2018) Data of adsorption of Basic Blue 41 dye from aqueous solutions by activated carbon prepared from filamentous algae. Data Br 21:1008–1013

Aharoni C, Ungarish M (1977) Kinetics of activated chemisorption. Part 2.—Theoretical models. J Chem Soc Faraday Trans 1 Phys Chem Condens Phases 73:456–464

Akkaya G, Özer A (2005) Biosorption of Acid Red 274 (AR 274) on Dicranella varia: Determination of equilibrium and kinetic model parameters. Process Biochem 40:3559–3568. https://doi.org/https://doi.org/10.1016/j.procbio.2005.03.048

An Y, Zheng H, Yu Z, et al (2020) Functioned hollow glass microsphere as a self-floating adsorbent: Rapid and high-efficient removal of anionic dye. J Hazard Mater 381:120971

Ashrafi M, Bagherian G, Chamjangali MA, Goudarzi N (2018) Application of artificial neural network and random forest methods for modeling simultaneous adsorption of safranin-O and methyl violet dyes onto modified pine cone powder. Desalin Water Treat 109:90–103

Azimvand J, Didehban K, Mirshokraie SA (2018) Safranin-O removal from aqueous solutions using lignin nanoparticle-g-polyacrylic acid adsorbent: Synthesis, properties, and application. Adsorpt Sci Technol 36:1422–1440

Chakma S, Moholkar VS (2011) Mechanistic features of ultrasonic desorption of aromatic pollutants. Chem Eng J 175:356–367. https://doi.org/https://doi.org/10.1016/j.cej.2011.09.123

Deng S, Li X, Fu H (2011) Acid violet 6B as a novel corrosion inhibitor for cold rolled steel in hydrochloric acid solution. Corros Sci 53:760–768. https://doi.org/http://dx.doi.org/10.1016/j.corsci.2010.11.002

Dubinin Mm (1960) The potential theory of adsorption of gases and vapors for adsorbents with energetically nonuniform surfaces. Chem Rev 60:235–241

Dubinin MM (1965) Modern state of the theory of volume filling of micropore adsorbents during adsorption of gases and steams on carbon adsorbents. Zhurnal Fiz Khimii 39:1305–1317

Freundlich HMF (1906) Over the adsorption in solution. J Phys Chem 57:1100–1107

Gougazeh M, Kooli F, Buhl J-C (2019) Removal Efficiency of Basic Blue 41 by Three Zeolites Prepared from Natural Jordanian Kaolin. Clays Clay Miner 67:143–153

Ho YS, McKay G (1999) Pseudo-second order model for sorption processes. Process Biochem 34:451–465. https://doi.org/https://doi.org/10.1016/S0032-9592(98)00112-5

Hossain MB, Brunton NP, Patras A, et al (2012) Optimization of ultrasound assisted extraction of antioxidant compounds from marjoram (Origanum majorana L.) using response surface methodology. Ultrason

Sonochem 19:582–590. https://doi.org/https://doi.org/10.1016/j.ultsonch.2011.11.001

Humelnicu I, Băiceanu A, Ignat M-E, Dulman V (2017) The removal of Basic Blue 41 textile dye from aqueous solution by adsorption onto natural zeolitic tuff: Kinetics and thermodynamics. Process Saf Environ Prot 105:274–287

Kamaru AA, Sani NS, Malek NANN (2016) Raw and surfactant-modified pineapple leaf as adsorbent for removal of methylene blue and methyl orange from aqueous solution. Desalin Water Treat 57:18836–18850. https://doi.org/10.1080/19443994.2015.1095122

Khodadoust S, Hadjmohammadi M (2011) Determination of N-methylcarbamate insecticides in water samples using dispersive liquid–liquid microextraction and HPLC with the aid of experimental design and desirability function. Anal Chim Acta 699:113–119. https://doi.org/https://doi.org/10.1016/j.aca.2011.04.011

Kooli F, Liu Y, Abboudi M, et al (2019) Waste Bricks Applied as Removal Agent of Basic Blue 41 from Aqueous Solutions: Base Treatment and Their Regeneration Efficiency. Appl Sci 9:1237

LAGERGREN, S. (1898) Zur theorie der sogenannten adsorption geloster stoffe. K Sven Vetenskapsakademiens Handl 24:1–39

Langmuir I (1918) The adsorption of gases on plane surfaces of glass, mica and platinum. J Am Chem Soc 40:1361–1403

LeFevre JW (2000) Isolating trans-Anethole from Anise Seeds and Elucidating Its Structure: A Project Utilizing One- and Two-Dimensional NMR Spectrometry. J Chem Educ 77:361. https://doi.org/10.1021/ed077p361

Li F, Bao Y, Chai J, et al (2010) Synthesis and Application of Widely Soluble Graphene Sheets. Langmuir 26:12314–12320. https://doi.org/10.1021/la101534n

Maddikeri GL, Pandit AB, Gogate PR (2012) Adsorptive Removal of Saturated and Unsaturated Fatty Acids Using Ion-Exchange Resins. Ind Eng Chem Res 51:6869–6876. https://doi.org/10.1021/ie3000562

Mahmoodi NM (2011) Equilibrium, Kinetics, and Thermodynamics of Dye Removal Using Alginate in Binary Systems. J Chem Eng Data 56:2802–2811. https://doi.org/10.1021/je101276x

Mahmoodi NM, Abdi J (2019) Nanoporous metal-organic framework (MOF-199): Synthesis, characterization and photocatalytic degradation of Basic Blue 41. Microchem J 144:436–442

Martins PF, Carmona C, Martinez EL, et al (2012) Evaluation of methyl chavicol concentration by different evaporation processes using central composite experimental design. Sep Purif Technol 98:464–471. https://doi.org/https://doi.org/10.1016/j.seppur.2012.08.009

453 Midathana VR, Moholkar VS (2009) Mechanistic Studies in Ultrasound-Assisted Adsorption for Removal of
454 Aromatic Pollutants. Ind Eng Chem Res 48:7368–7377. https://doi.org/10.1021/ie900049e
455 Mullerova S, Baldikova E, Prochazkova J, et al (2019) Magnetically modified macroalgae Cymopolia barbata
456 biomass as an adsorbent for safranin O removal. Mater Chem Phys 225:174–180
457 Noroozi B, Sorial GA (2013) Applicable models for multi-component adsorption of dyes: A review. J Environ
458 Sci 25:419–429. https://doi.org/https://doi.org/10.1016/S1001-0742(12)60194-6
459 Pan B, Pan B, Zhang W, et al (2009) Development of polymeric and polymer-based hybrid adsorbents for
460 pollutants removal from waters. Chem Eng J 151:19–29.
461 https://doi.org/https://doi.org/10.1016/j.cej.2009.02.036
462 Pizarro C, Sáenz-González C, Pérez-del-Notario N, González-Sáiz JM (2012) Development of an ultrasound-
463 assisted emulsification–microextraction method for the determination of the main compounds causing cork
464 taint in wines. J Chromatogr A 1229:63–71. https://doi.org/https://doi.org/10.1016/j.chroma.2012.01.033
465 Pushpa T B, Josephraj J, Saravanan P, Ravindran G (2019) Biodecolorization of Basic Blue 41 using EM based
466 Composts: Isotherm and Kinetics. ChemistrySelect 4:10006–10012
467 Radushkevich L V (1949) SORBTSIYA I STRUKTURA AKTIVNYKH UGLEI. 7. POTENTSIALNAYA
468 TEORIYA ADSORBTSII I STRUKTURA AKTIVNYKH UGLEI. ZHURNAL Fiz KHIMII 23:1410–1420
469 Reddy YS, Magdalane CM, Kaviyarasu K, et al (2018) Equilibrium and kinetic studies of the adsorption of acid
470 blue 9 and Safranin O from aqueous solutions by MgO decked FLG coated Fuller's earth. J Phys Chem
471 Solids 123:43–51
472 Regti A, Laamari MR, Stiriba S-E, El Haddad M (2017) Removal of Basic Blue 41 dyes using Persea americana-
473 activated carbon prepared by phosphoric acid action. Int J Ind Chem 8:187–195
474 Saeid K, Mehrorang G (2013) Optimization of dispersive liquid–liquid microextraction with central composite
475 design for preconcentration of chlordiazepoxide drug and its determination by HPLC-UV. J Sep Sci
476 36:1734–1742. https://doi.org/10.1002/jssc.201300085
477 Shaban M, Abukhadra MR, Mohamed AS, et al (2018) Synthesis of mesoporous graphite functionalized by
478 nitrogen for efficient removal of safranin dye utilizing rice husk ash; equilibrium studies and response
479 surface optimization. J Inorg Organomet Polym Mater 28:279–294
480 Shariati S, Faraji M, Yamini Y, Rajabi AA (2011) Fe3O4 magnetic nanoparticles modified with sodium dodecyl
481 sulfate for removal of safranin O dye from aqueous solutions. Desalination 270:160–165.
482 https://doi.org/https://doi.org/10.1016/j.desal.2010.11.040

Sharifpour E, Ghaedi M, Nasiri Azad F, et al (2018) Zinc oxide nanorod-loaded activated carbon for ultrasound-assisted adsorption of safranin O: Central composite design and genetic algorithm optimization. Appl Organomet Chem 32:e4099

Shelar-Lohar G, Joshi S (2019) Amidoximated functionalized sodium alginate graft copolymer: An effective adsorbent for rapid removal of cationic dyes. Mater Today Proc

Tan TCN, Sen TK (2020) Aqueous-phase methylene blue (MB) dye removal by mixture of eucalyptus bark (EB) biomass and kaolin clay (KC) adsorbents: kinetics, thermodynamics, and isotherm modeling. Sep Sci Technol 55:1036–1050

Tempkin MI, Pyzhev V (1940) Kinetics of ammonia synthesis on promoted iron catalyst. Acta Phys Chim USSR 12:327

Thompson LH, Doraiswamy LK (1999) Sonochemistry: Science and Engineering. Ind Eng Chem Res 38:1215–1249. https://doi.org/10.1021/ie9804172

Weber WJ, Morris JC (1963) Kinetics of adsorption on carbon from solution. J Sanit Eng Div 89:31–60

Figures

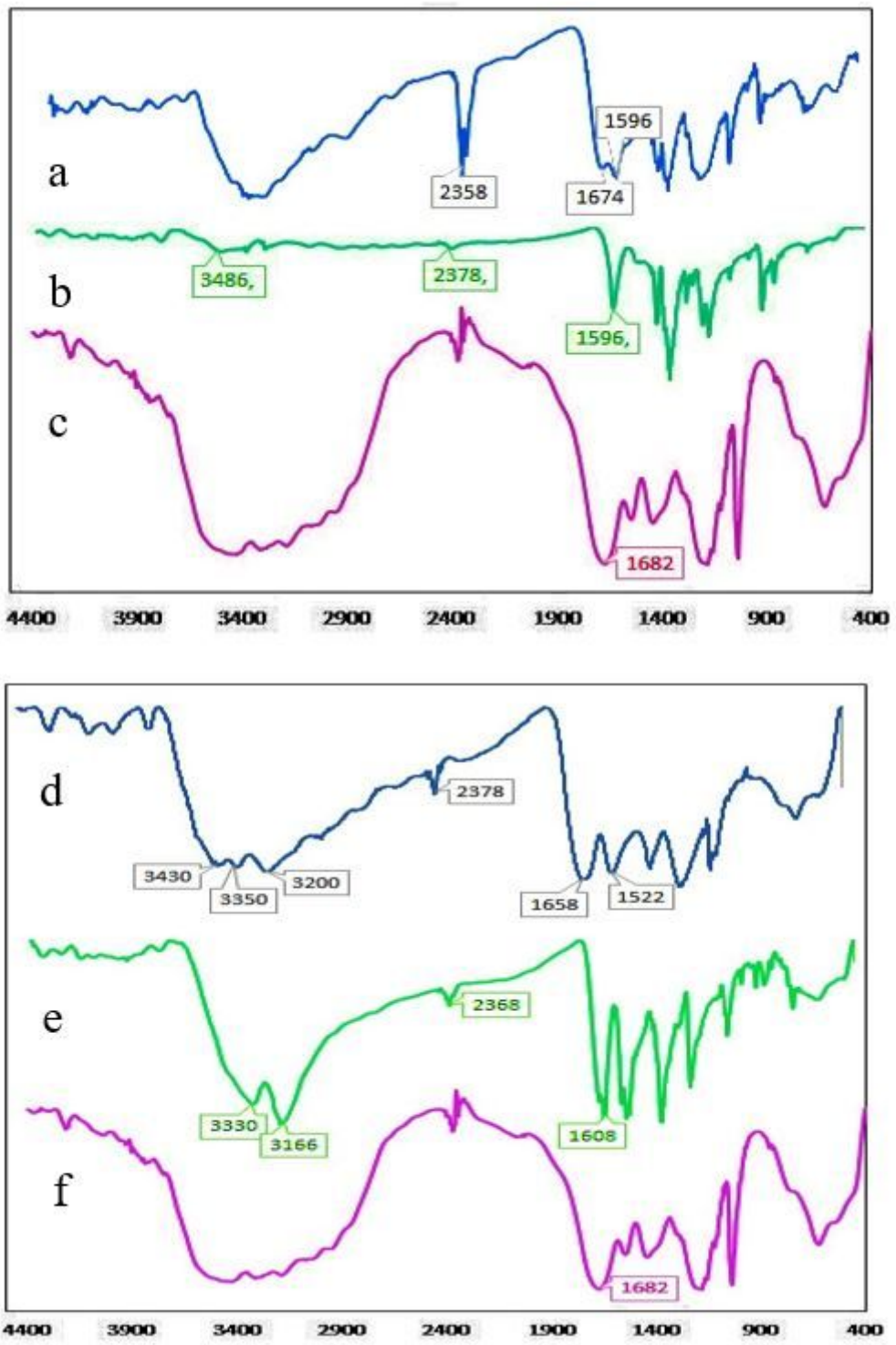

Figure 1

FT-IR (KBr) for the developed adsorbent. (a) adsorbed BB on PAA- SO3H (b) BB, (c) PAA- SO3H adsorbent, (d) adsorbed SO on PAA- SO3H (e) SO, (f) PAA- SO3H adsorbent.

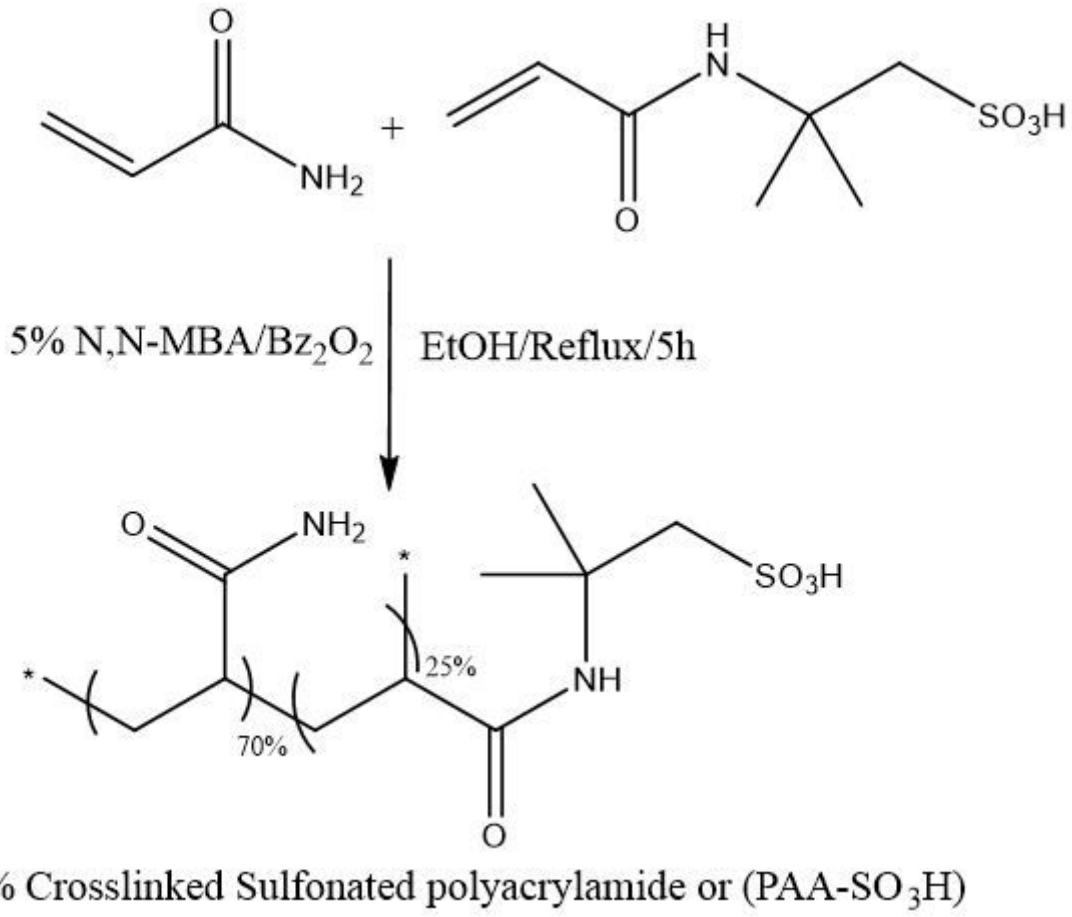

Figure 2

Preparation of sulfonated polyacrylamide via transamidation reaction

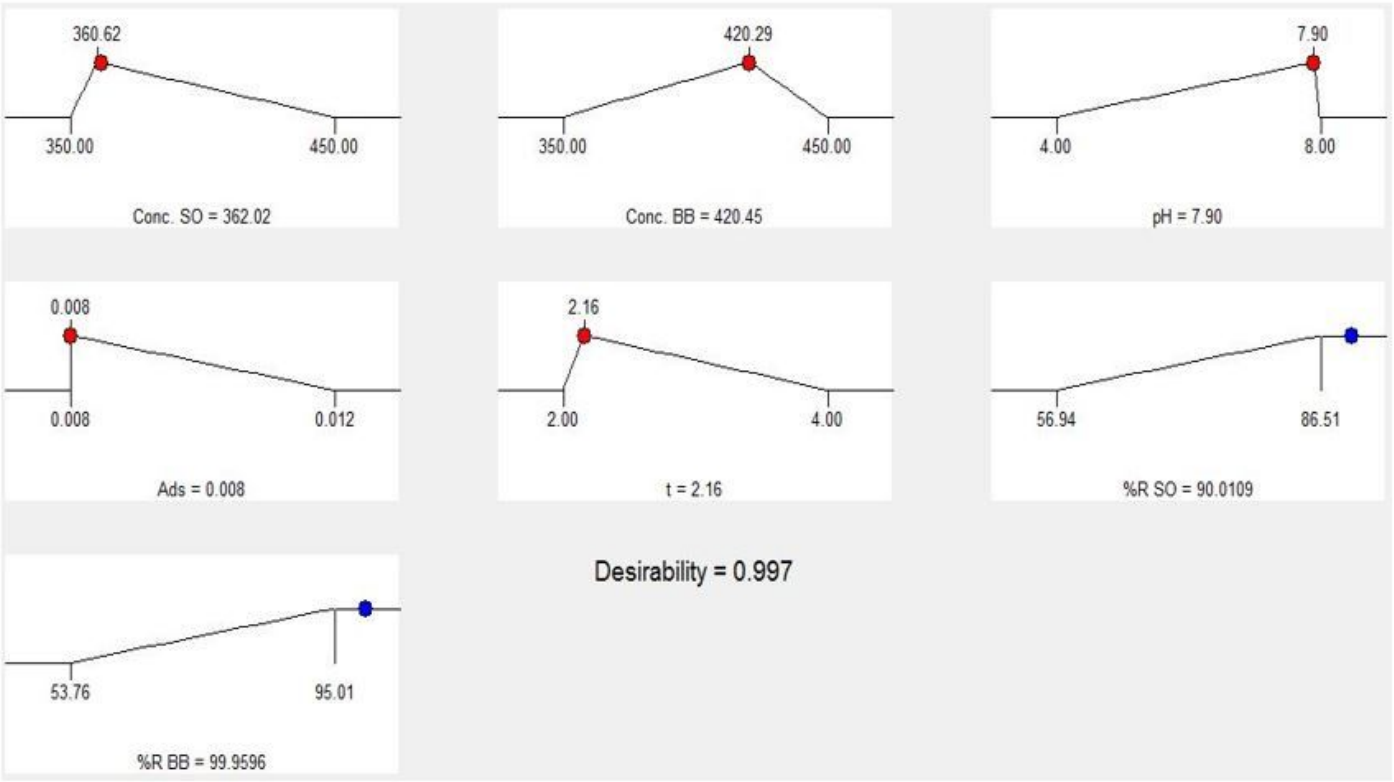

Figure 3

Optimization plot of factors.

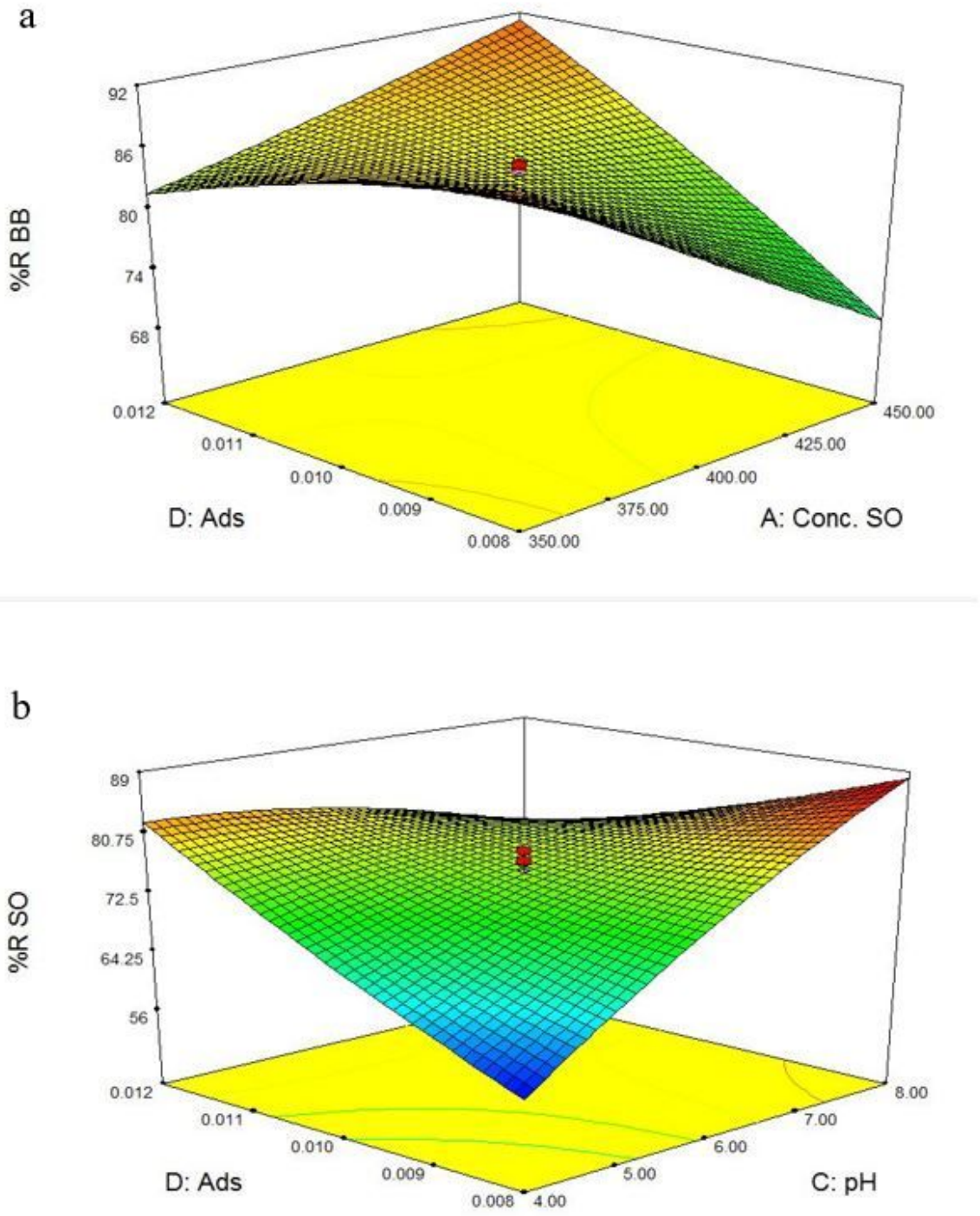

Figure 4

Response surfaces for the 25 central composite designs for simultaneous of SO and BB. a) SO concentration and adsorbent, (b) pH and adsorbent.